NANO LETTERS

pubs.acs.org/NanoLett

Letter

Magnetic Interactions Between Radical Pairs in Chiral Graphene Nanoribbons

Tao Wang,*,⊥ Sofia Sanz,⊥ Jesús Castro-Esteban, James Lawrence, Alejandro Berdonces-Layunta, Mohammed S. G. Mohammed, Manuel Vilas-Varela, Martina Corso, Diego Peña,* Thomas Frederiksen,* and Dimas G. de Oteyza*

Cite This: *Nano Lett.* 2022, 22, 164−171

Read Online

ACCESS | Metrics & More | Article Recommendations | Supporting Information

ABSTRACT: Open-shell graphene nanoribbons have become promising candidates for future applications, including quantum technologies. Here, we characterize magnetic states hosted by chiral graphene nanoribbons (chGNRs). The substitution of a hydrogen atom at the chGNR edge by a ketone effectively adds one p_z electron to the π-electron network, producing an unpaired π-radical. A similar scenario occurs for regular ketone-functionalized chGNRs in which one ketone is missing. Two such radical states can interact via exchange coupling, and we study those interactions as a function of their relative position, which includes a remarkable dependence on the chirality, as well as on the nature of the surrounding ribbon, that is, with or without ketone functionalization. Besides, we determine the parameters whereby this type of system with oxygen heteroatoms can be adequately described within the widely used mean-field Hubbard model. Altogether, we provide insight to both theoretically model and devise GNR-based nanostructures with tunable magnetic properties.

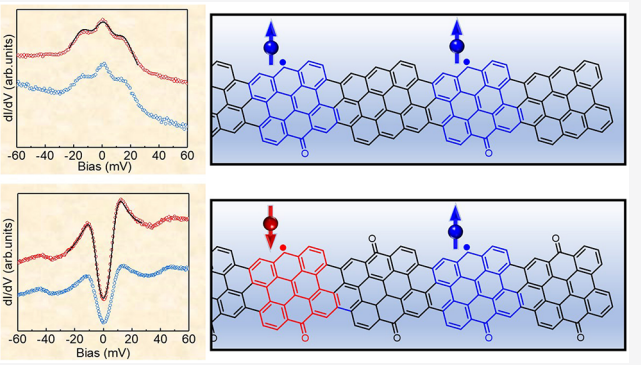

KEYWORDS: *magnetism, spin interaction, graphene nanoribbon, heteroatom substitution, scanning tunneling microscopy, density functional theory, mean-field Hubbard model*

Magnetic carbon nanostructures exhibit attractive properties that differentiate them from the conventional magnetic systems relying on d or f states, like a weaker spin−orbit coupling and a larger spin delocalization.[1−5] The open-shell character and the corresponding magnetic properties may appear in graphene nanoflakes (GNFs) and nanoribbons (GNRs) with certain topologies for a number of reasons. First, as predicted by Lieb's theorem[6] sublattice imbalance in a bipartite lattice leads to a net spin inside the nanographene that occurs, for example, in triangulene.[7] Even with balanced sublattices, topological frustration in GNFs may hinder the pairing of all p_z electrons and result in open-shell structures.[8] In addition, if the Coulomb repulsion between valence electrons is comparable to the band gap between molecular frontier orbitals, it can prompt the system to host singly occupied orbitals.[9−13] Finally, a net spin can be introduced to GNFs and GNRs by simply adding/removing an odd number of π-electrons into/from the system.[14] Besides charge transfer scenarios,[15,16] this can also be achieved by the insertion of odd-membered rings,[17−20] by an sp^2 to sp^3 rehybridization as driven, for example, by hydrogenation,[10,21] or by heteroatom substitutions.[22] The former two approaches have been increasingly employed[10,17−20,23] but only few examples elucidate the latter one[24] though with many theoretical predictions.[22,25,26]

The synthesis and characterization of graphene π-magnetism has seen great advances thanks to the recent development of on-surface synthesis.[10,14−16,18,19,21,24,27−37] The topologies of GNFs and GNRs can be precisely tuned by the rational design of precursor molecules. Because of their delocalized π-magnetism, magnetic GNFs and GNRs are ideal candidates for the construction of interacting electron spin systems. Most of the reported works are focused on the interactions between radicals on GNFs,[14,37] whereas the engineering of exchange-coupled spins on extended systems like GNRs, though highly desired, is more scarce.[24,28,38]

Here, we report the generation of net spins on chiral GNRs (chGNRs) by ketone functionalization as shown in Figure 1a.

Received: September 15, 2021
Revised: December 3, 2021
Published: December 22, 2021

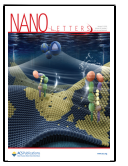

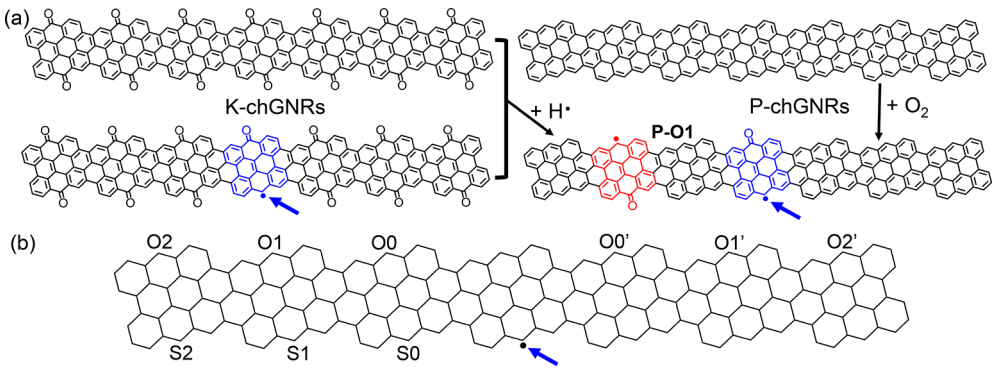

Figure 1. Synthesis and nomenclature of radicals and radical pairs. (a) Schematic drawing for the fabrication of magnetic chGNRs. A π-radical is introduced into chGNRs by the addition/removal of an oxygen into/from P-/K-chGNRs. (b) Labels for the radical pairs in chGNRs. Taking the radical marked with a blue arrow as the reference, each pair is labeled depending on the position of the second π-radical.

Replacing a CH at the pristine chGNR edge by a C═O (carbonyl) adds one π-electron to the system. As a result, the odd number of total electrons causes the appearance of a π-radical. The same is applicable for regularly ketone-functionalized chGNRs[39] if a C═O is replaced by a CH. The introduction of a second radical may either maintain the system's open-shell character or result in their hybridization into a closed-shell structure.[33,37] On the basis of the above, a variety of radical pairs with different geometries were analyzed in our experiments. Combining scanning tunneling microscopy (STM) with theoretical calculations, we reveal how their relative location, the chemical structure of the units surrounding the two radicals and the chirality itself, all influence the spin interactions.

The generation of radical states in chGNRs is schematically displayed in Figure 1a and starts from the readily described synthesis of pristine (P-) and ketone-functionalized (K-) chGNRs on Au(111).[39,40] In the case of K-chGNRs, a few defective ribbons with one or more missing oxygen atoms normally coexist with intact ribbons.[39] The substitution of an oxygen by a hydrogen atom makes the total number of p_z electrons an odd number, thus producing an unpaired π-radical, as indicated by the blue arrow in Figure 1a. In turn, the addition of an oxygen atom to an otherwise P-chGNRs effectively adds one p_z electron and equally brings in a radical. This can be achieved either by exposing P-chGNRs to O_2 and postannealing,[41] or removing most of the ketones of K-chGNRs by exposing them to atomic hydrogen and postannealing.[39] Using these procedures, P- and K-chGNRs with single radicals and with radical pairs were produced. Unfortunately, attempts to controllably remove ketone groups by tip manipulation and thereby create radicals at predesigned positions were unsuccessful. We use the following nomenclature to refer to different radical pairs. Taking the radical marked with the blue arrow in Figure 1b as reference, the other labels denote the position of the second radical (Figure 1b). S/O represents the two radicals of a pair located at the same/opposite sides of a chGNR. The following number shows how many precursor units separate a radical pair. A′-mark is used to distinguish the differing configurations resulting from the ribbon's chirality. Finally, P- denotes P-chGNRs in which the radicals are caused by additional ketones and K- denotes K-chGNRs with radicals associated with missing ketones. An example P-O1 radical pair is shown in Figure 1a.

Figure 2a presents the bond-resolving (BR) STM image of a K-chGNR with a single defect using a CO-functionalized

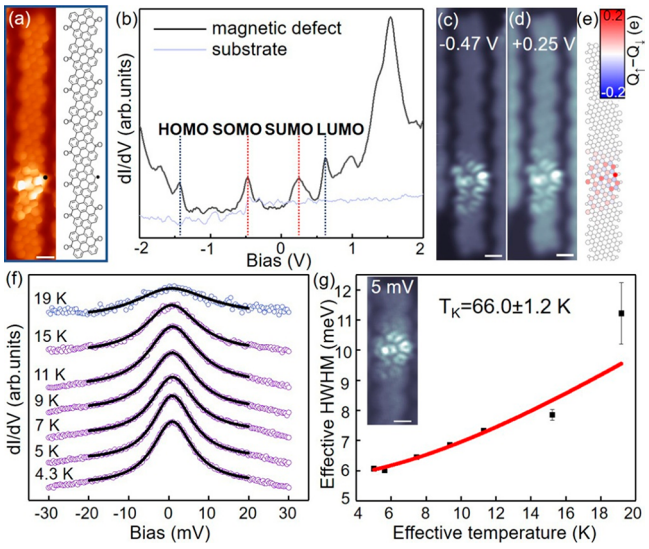

Figure 2. Characterization of single radicals. (a) Constant-height BR-STM image of a K-chGNR with single defect (V = 5 mV), together with the corresponding chemical structure. (b) dI/dV spectra at the marked position in (a, black line) and the bare Au(111) substrate (gray line), V_{rms} = 20 mV. (c,d) Constant-height dI/dV maps recorded at V = −0.47 and 0.25 V, respectively. V_{rms} = 20 mV. (e) DFT calculated spin density distribution in K-chGNR with single defect. (f) Temperature dependence of the Kondo resonance. All of the spectra are fitted by a Frota function. (g) Extracted HWHM of the Kondo resonances as a function of temperature, fitted by the Fermi-liquid model. The inset shows a Kondo map measured at 5 mV. Scale bars: 0.5 nm.

probe,[42] along with the associated chemical structure. At the low bias value used for BR-STM, the unit cell with a missing ketone exhibits brighter contrast, implying the existence of low-energy states. Figure 2b shows the differential conductance spectrum (dI/dV) taken at the marked position in Figure 2a. Apart from the highest occupied and lowest unoccupied molecular orbitals (HOMO and LUMO) of a K-chGNR at −1.45 and 0.65 V, associated with the reported valence and conduction band onsets,[39] two in-gap states are clearly visible at −0.47 and 0.25 V. The same local density of states (LDOS) distribution at these two energies in dI/dV maps supports their common origin from the singly occupied/unoccupied molecular orbitals (SOMO/SUMO), separated by a 0.72 eV Coulomb gap.[36] In line with the experiments, the spin density calculated for this structure with density functional theory

https://doi.org/10.1021/acs.nanolett.1c03578
Nano Lett. 2022, 22, 164−171

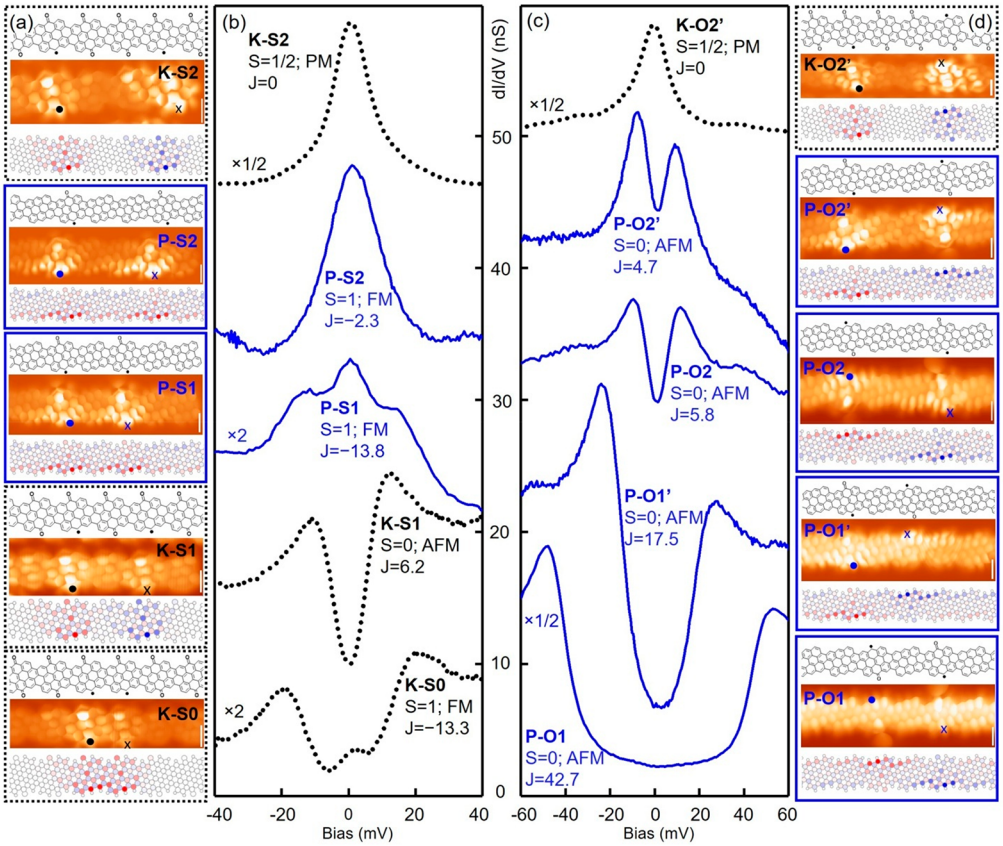

Figure 3. Characterizations of radical pairs. (a,d) BR-STM images (V = 5 mV) of experimentally obtained radical pairs at the same (a) and opposite sides (d) on P- and K-chGNRs, together with the chemical structure and DFT calculated spin-polarized LDOS for each case (ground states). (b,c) dI/dV spectra measured at the marked positions in STM images (see comparative spectra at the position of the second radical marked with an x in the Figure S5. The blue solid and black dotted curves refer to radical pairs on P- and K-chGNRs, respectively. P-O1 shows the original signal and other spectra were vertically shifted to match the positions of STM images. Some of the spectra were additionally scaled as marked. Total spin and coupling strength are shown for each case, where PM, FM, and AFM stand for paramagnetic, ferromagnetic and antiferromagnetic coupling, respectively. Lock-in amplitude: 2 mV for P-O1, 1.5 mV for K-S0, 1 mV for other cases. Scale bars: 0.5 nm.

(DFT) with SIESTA[43,44] (Figure 2e and Figure S1 in Supporting Information) distributes mostly over the "defective" unit cell but extends slightly to the adjacent ones with a clear chirality-driven asymmetry. Evidence of this system's net spin S = 1/2 is detected as a zero-bias peak in the low-energy dI/dV spectra (Figure 2f). It broadens anomalously fast with temperature and can thus be attributed to a Kondo resonance.[14,45] The half width at half-maximum (HWHM) of the temperature-dependent spectra, as extracted from fits to a Frota function[46] (Figure 2f), are further fitted to the Fermi-liquid model[47] (Figure 2g) and result in a Kondo temperature of 66 K. The identical spin distribution of the Kondo map obtained at 5 mV (Figure 2g inset) and of the SOMO/SUMO (Figure 2c,d) further corroborates the origin of the spin density in the SOMO.

An equivalent characterization of a single magnetic defect in P-chGNR is presented in Figure S2. Compared to the K-chGNR case, the SOMO and the associated spin density in P-chGNR show a much more limited contribution on the ketone and mostly distribute over the pristine side of the defective unit cell. The smaller bandgap of P-chGNR as compared to K-chGNR (~0.7 vs ~2.1 eV),[39,48] causes a stronger hybridization of the radical states with the frontier molecular orbitals, resulting in a notably more extended distribution into neighboring unit cells (though with a similar chirality-driven asymmetry) and consequently a lower Coulomb gap of only 0.35 eV.

Next, we focus on chGNRs with radical pairs. Whereas a hybridization of the two radicals may result in a closed-shell ground state with a doubly occupied HOMO, the system can also remain open-shell with the associated SOMOs, if the hybridization energy is lower than the Coulomb repulsion between the corresponding electrons.[33,37] Our DFT calculations (Figure S1) predict two radicals in closest proximity but opposite GNR sides (i.e., the O0 and O0′ cases in both types of chGNRs) to hybridize into a closed-shell ground state, while all of the other radical combinations show open-shell ground states. The experimentally observed P-O0, P-O0′, and K-O0′ cases confirm their closed-shell character and are displayed in Figure S3 with HOMOs and LUMOs exhibiting distinct LDOS distributions as opposed to the similar appearance expected from SOMO and SUMO.

For the open-shell structures, the exchange interaction between a radical pair can be experimentally accessed from inelastic spin-flip excitations in scanning tunneling spectroscopy.[14] The low-energy dI/dV spectra of radical pairs with a S = 1 triplet ground state may exhibit three features: an underscreened Kondo resonance at Fermi level and two side steps symmetrically positioned around the Fermi level. The latter are associated with inelastic triplet-to-singlet spin-flip excitations,[15,18] and in contrast to their energetic alignment

https://doi.org/10.1021/acs.nanolett.1c03578
Nano Lett. 2022, 22, 164−171

their intensities may display asymmetries as a result of lacking particle-hole symmetry (that is, the singly occupied orbital is closer to E_F than the singly unoccupied state or vice versa), spin-polarized tips, and so forth.[10,49] In contrast, the dI/dV spectra of radical pairs with a $S = 0$ singlet ground state exhibit only the two singlet-to-triplet side steps.[18,19,36,37] As the exchange interaction between the radicals becomes sufficiently weak, equaling singlet and triplet energies, the radicals respond independently from one another and may display only a Kondo resonance. The geometries of the experimentally addressed radical pairs are determined from the BR-STM images displayed in Figure 3a,d, along with their spin densities as calculated with DFT. The associated low-energy dI/dV spectra are shown in Figure 3b,c. In agreement with the above, further confirmed with fits to the spectra (Figure S5) with a perturbative approach up to third order for two coupled $S = 1/2$ systems using the code from Ternes that is explained in detail in ref 49, we conclude the exchange coupling energies and relative alignments for each radical pair as summarized in Table 1. Table 1 also includes the values obtained from theoretical calculations. The good match of the DFT results with the experiments underlines the predictive power of the calculations on radical pair geometries not accessed experimentally.

Table 1. Exchange-Interaction Strength J (in meV) Obtained from Experiments and Theoretical Calculations for Multiple Radical Pairs[a,b]

type	experiment	DFT	MFH-TB(1)	MFH-TB(2)
P-S0		−31.4	−44	−23.2
P-S1	−13.8	−18.4	−15.5	−12.8
P-S2	−2.3	−11	−7.2	−6.4
P-O0	CS	CS	CS	CS
P-O0′	CS	CS	108	CS
P-O1	42.7	35.8	29	28.8
P-O1′	17.5	28	21.4	20.4
P-O2	5.8	11.3	7.8	6.9
P-O2′	4.7	11.8	7.8	7.1
K-S0	−13.3	−24	−50.9	−19
K-S1	6.2	6.4	−6.6	2.1
K-S2	0	0.4	−0.5	0.1
K-O0		CS	CS	CS
K-O0′	CS	CS	109.1	CS
K-O1		29.1	14.4	20.9
K-O1′		−0.5	2.7	0
K-O2		0.1	0.9	0.5
K-O2′	0	0.7	0.3	0

[a]Positive (negative) J values indicate preferred antiferromagnetic (ferromagnetic) alignment. [b]CS denotes closed-shell structure.

Focusing on the exchange coupling J, it scales inversely with the spatial separation for both P- and K-chGNRs cases. That is, radical pairs separated by less unit cells show larger J values due to the greater overlap of the radical states' wave functions and the associated spin density (Figure 3a,d). Interestingly, J shows a remarkable dependence on the chirality, as observed experimentally with P-O1 and P-O1′ and predicted theoretically also for K-O1 and K-O1′ (Table 1). The chirality-driven asymmetric extension of the SOMO wave function (and of the associated spin density) into neighboring unit-cells strongly affects their overlap. For example, whereas the spin density of radical states in P-O1 mostly extends toward the central unit between the radical pairs, it dominantly extends away from each other in P-O1′ (Figure 3d). As a consequence, the former shows a much stronger exchange coupling than the latter (42.7 vs 17.5 meV). The exchange coupling strength also varies substantially with the nature of the surrounding GNR, as exemplified here with the presence or absence of the edge functionalization by ketones. Radical states in K-chGNRs extend much less than those in P-chGNRs, promoting in the latter a larger overlap and thus larger J for the same radical pair geometry (Figure 3 and Table 1).

As for the spin's relative alignment, a generally applicable assumption that relies on the preferred antiferromagnetic alignment of electrons in chemical bonds is that, for alternant graphene nanostructures, each of the two sublattices hosts p_z electrons with spin up or down, respectively. Since the ketone group is also sp^2 hybridized, it adds one p_z electron to the system and can to a first approximation be considered as an additional p_z site on its corresponding sublattice. The atoms at same edges of the chGNRs belong to the same sublattice, whereas the atoms at the opposite edge belong to the other sublattice. A radical pair located at the same/opposite side is therefore expected to be ferromagnetically (FM)/antiferromagnetically (AFM) aligned. All experimentally measured radical pairs match this prediction, except K-S1 (AFM ground state; Table 1).

For the conductance spectrum of K-S1, one could argue that the Kondo peak expected from a FM alignment is not visible because its intensity is much lower than that of the spin flip steps (as occurs, e.g., in K-S0, Figure 3b), and its width is comparable to J. In fact, the spectrum can be fitted using Ternes' code[49] assuming an FM alignment. However, to do so, the tip−sample transmission function represented by the T_0^2 parameter required an anomalously large value. Since we did not change the STM tip during the whole experiment and used comparable tip−sample distances as defined by the STM feedback parameters, it is natural to expect that T_0^2 should be similar for all the spin-coupling scenarios. As shown in Figure S6, whereas all the other fits rendered comparable T_0^2 values, a FM alignment for the K-S1 case required a T_0^2 value an order of magnitude higher and clearly out of the dispersion range, suggesting a preferred AFM alignment of the K-S1 radical pair.

This counterintuitive spin alignment for the K-S1 case is confirmed with DFT calculations, which predict the AFM alignment to be energetically favored. We have additionally performed mean-field Hubbard (MFH) calculations[50] on this same system, given its greater simplicity and successful application to many open-shell carbon nanostructures.[14,37] As discussed earlier, the extra p_z electron on the sp^2 hybridized ketone was first considered as an additional p_z site taken to be identical to a carbon p_z orbital. Doing so, MFH calculations with the third nearest-neighbor tight-binding model (3NN-TB) predict a FM ground state for K-S1, in line with the intuitive expectations for radical states on the same ribbon's side but against DFT and experiments (henceforth we call this model MFH-TB(1)). In a counter-experiment, we performed DFT calculations for another system which is more equivalent to a simulation performed with MFH-TB(1), namely a chGNR with methylidene groups (i.e., C═CH_2) instead of carbonyl (C═O). In this case, the DFT results agree with the intuitive expectations and with the MFH-TB(1), predicting a preferred FM alignment and even a comparable J value (CH_2-S1 in Figure 4a). It follows that the surprising AFM alignment is unequivocally related to the oxygen atom rather than to the

https://doi.org/10.1021/acs.nanolett.1c03578
Nano Lett. 2022, 22, 164−171

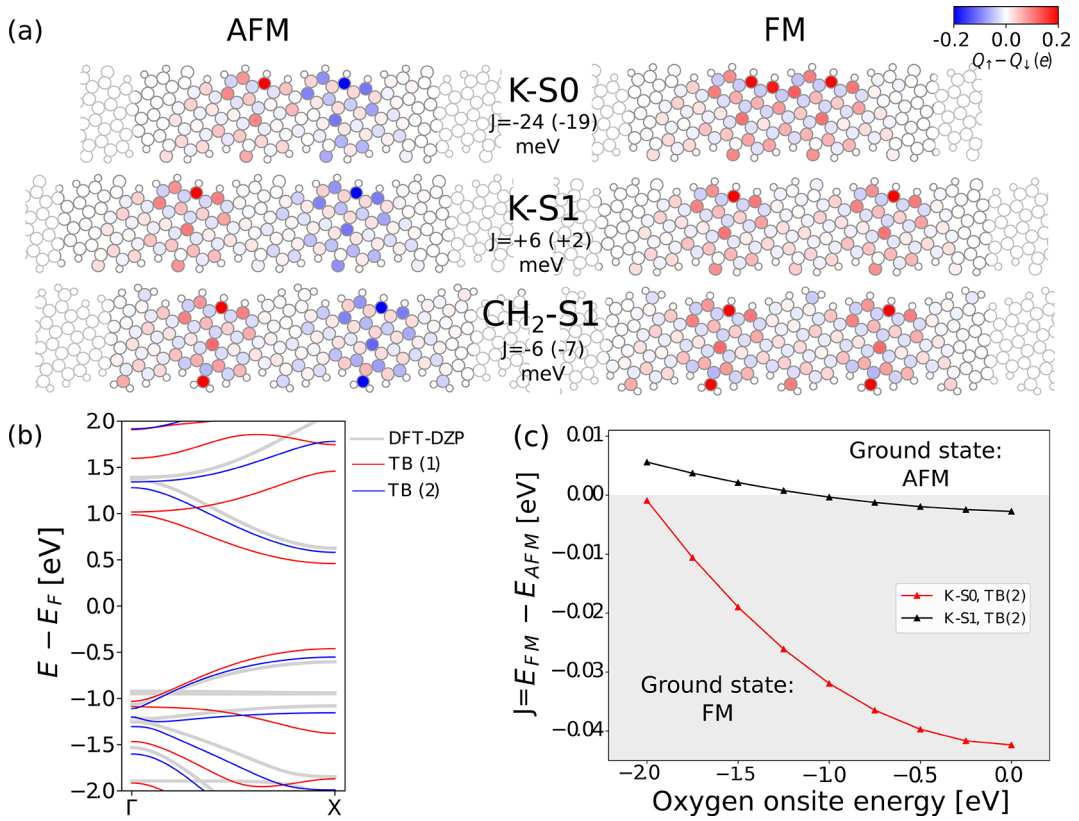

Figure 4. Modeling of radical pairs. (a) Spin-polarized LDOS distribution of radical states as calculated by DFT and J (MFH-TB(2) values are shown in parentheses) in K-S0, K-S1, and CH_2-S1 (all oxygen atoms are replaced by CH_2), respectively. (b) Band structures of intact K-chGNR, acquired from DFT, MFH-TB(1), and MFH-TB(2), respectively. (c) MFH-TB calculated J in K-S0 and K-S1 as a function of oxygen onsite energy in TB(2). The onsite Coulomb repulsion in MFH was set to U = 3 eV.

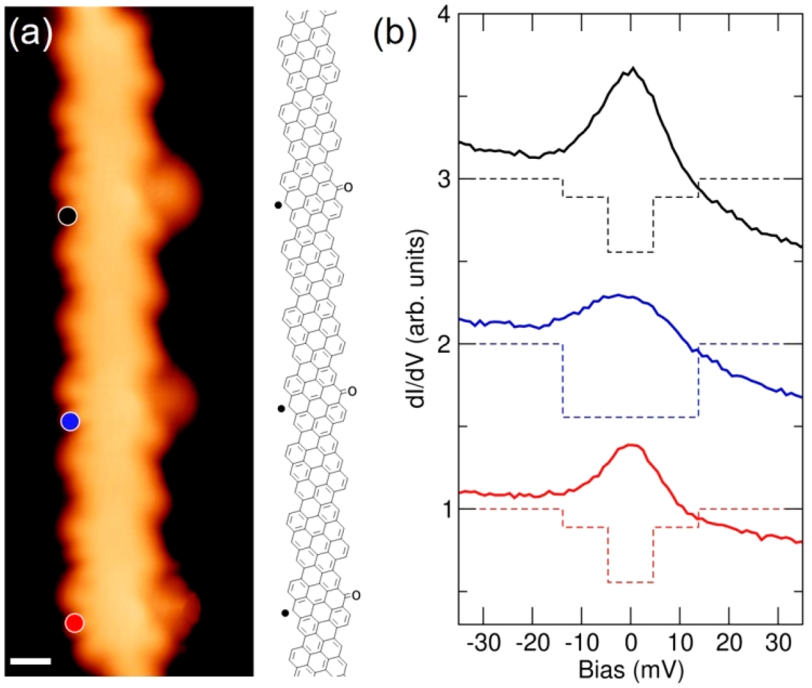

Figure 5. (a) STM image (U = −100 mV; I = −1 nA) showing a P-chGNR with three P-S2 radicals in a row, together with the corresponding chemical structure. The scale bar is 5 Å. (b) Vertically offset dI/dV spectra (solid lines) obtained at the marked positions in (a), along with the simulated inelastic electron tunneling spectroscopy (dashed lines) for this three-radical spin system. The exchange energy J = −2.3 meV, as derived from P-S2 in experiments, is used for the simulation.

https://doi.org/10.1021/acs.nanolett.1c03578
Nano Lett. 2022, 22, 164−171

mere presence of an extra p_z electron there, exposing insufficient chemical detail in our simple MFH-TB(1) approach.

In an attempt to make the simple MFH calculations also applicable to these more complicated systems including heteroatoms, we have included modified TB parameters (hopping amplitude and on-site energy) for the oxygen heteroatoms in what we call the model MFH-TB(2). To determine the most appropriate parameters, we compare the calculated band structures obtained from DFT for fully ketone-functionalized chGNRs to those obtained with our MFH-TB models (Figure 4b). An improvement of the TB model can be obtained with MFH-TB(2) maintaining for carbon atoms the nearest-neighbor hopping amplitude and on-site energies of 2.7 and 0 eV, respectively, but changing the values to 3.8 and −1.5 eV for oxygen atoms bonded to carbon. Qualitatively the increased hopping amplitude on the C═O bonds can be directly related to its shorter length and the nonzero on-site energy to the increased electronegativity of oxygen. The exchange coupling in radical pairs (both strength and sign) is strongly affected by these two parameters, as depicted for the on-site energy in Figure 4c for K-S0 and K-S1. Applying this optimized model now correctly predicts a preferred AFM alignment for K-S1. Furthermore, MFH-TB(2) also corrects the other wrong predictions of the MFH-TB(1) model, as is the open-shell character of the P-O0′ and K-O0′ radical pairs and provides for all calculated structures J values very similar to DFT calculations (see Table 1). Altogether, we hereby provide a simple yet accurate parametrization to model these more complex systems beyond pure hydrocarbon structures.

It is worth noting that the insight provided in this work about the pairwise interaction between radicals can be extended also to systems with an increasing number of spins and ultimately even to spin chains. By way of example, three P-S2 radical states in a row (Figure 5a) reveal a clearly broader zero-bias resonance at the central radical (blue data, HWHM = 9 meV, Figure 5b) as compared to the two outer ones (black and red data, HWHM = 7 meV). For this geometry, the three spins are ferromagnetically coupled, leading to a ground state $S = 3/2$ with two distinct spin-flip excitations to the $S = 1/2$ manifold. Theoretical simulations of the corresponding inelastic dI/dV features (Figure 5b, dashed lines) reveal that only the high-energy excitation contributes at the central radical, whereas the outer sites exhibit predominantly the low-energy steps. Although a clear identification of these inelastic transitions in our spectra is hindered by the low energies involved, along with a relatively broad Kondo signal, these calculations are consistent with the experiment and the broader peak at the central spin (Figure 5b). This finding is also in line with the previous work from DiLullo et al.,[51] where the central site on a molecular Kondo chain was found to exhibit a larger resonance width than those at the termini. Although the spins in that case were aligned antiferromagnetically, the same argument actually holds.

In summary, we have characterized the magnetic interactions between radical pairs of diverse geometries hosted by two different types of chGNRs, with and without ketone functionalization at their edges. As confirmed by both experiments and theoretical calculations, the exchange coupling between two radicals shows remarkably large variations depending on their relative location on the same or opposite sides of the GNRs, on the spatial distance between them, on the chiral asymmetry, as well as on the structure of the GNR surrounding the magnetic state. These results thus provide valuable information on the potential use in the design of graphene-based spin chains and networks with tunable magnetic structures. Furthermore, we demonstrated their modeling by the widely used MFH approximation through a minimal extension to these systems of increased complexity including oxygen heteroatoms, which may greatly expedite the understanding and engineering of GNR-based structures in the future.

■ ASSOCIATED CONTENT

Supporting Information

The Supporting Information is available free of charge at https://pubs.acs.org/doi/10.1021/acs.nanolett.1c03578.

Detailed methods of both experiments and calculations; spin density distributions of radical states on magnetic chGNRs by theoretical calculations; characterization of the magnetism of a P-chGNR with a single defect; closed-shell structures; Kondo peak comparison between K-chGNR with single defect and K-S2, K-O2′; simulations of the dI/dV spectra from radical pairs (PDF)

■ AUTHOR INFORMATION

Corresponding Authors

Tao Wang − *Donostia International Physics Center, 20018 San Sebastián, Spain; Centro de Fisica de Materiales CFM/MPC, CSIC-UPV/EHU, 20018 San Sebastián, Spain;* orcid.org/0000-0002-6545-5028; Email: taowang@dipc.org

Diego Peña − *Centro Singular de Investigación en Química Biolóxica e Materiais Moleculares (CiQUS) and Departamento de Química Orgánica, Universidade de Santiago de Compostela, 15782 Santiago de Compostela, Spain;* orcid.org/0000-0003-3814-589X; Email: diego.pena@usc.es

Thomas Frederiksen − *Donostia International Physics Center, 20018 San Sebastián, Spain; Ikerbasque, Basque Foundation for Science, 48013 Bilbao, Spain;* orcid.org/0000-0001-7523-7641; Email: thomas_frederiksen@ehu.eus

Dimas G. de Oteyza − *Donostia International Physics Center, 20018 San Sebastián, Spain; Centro de Fisica de Materiales CFM/MPC, CSIC-UPV/EHU, 20018 San Sebastián, Spain; Ikerbasque, Basque Foundation for Science, 48013 Bilbao, Spain;* orcid.org/0000-0001-8060-6819; Email: d_g_oteyza@ehu.eus

Authors

Sofia Sanz − *Donostia International Physics Center, 20018 San Sebastián, Spain;* orcid.org/0000-0002-2792-2721

Jesús Castro-Esteban − *Centro Singular de Investigación en Química Biolóxica e Materiais Moleculares (CiQUS) and Departamento de Química Orgánica, Universidade de Santiago de Compostela, 15782 Santiago de Compostela, Spain*

James Lawrence − *Donostia International Physics Center, 20018 San Sebastián, Spain; Centro de Fisica de Materiales CFM/MPC, CSIC-UPV/EHU, 20018 San Sebastián, Spain;* orcid.org/0000-0001-5503-8661

Alejandro Berdonces-Layunta − *Donostia International Physics Center, 20018 San Sebastián, Spain; Centro de Fisica*

https://doi.org/10.1021/acs.nanolett.1c03578
Nano Lett. 2022, 22, 164−171

de Materiales CFM/MPC, CSIC-UPV/EHU, 20018 San Sebastián, Spain

Mohammed S. G. Mohammed − *Donostia International Physics Center, 20018 San Sebastián, Spain; Centro de Fisica de Materiales CFM/MPC, CSIC-UPV/EHU, 20018 San Sebastián, Spain*

Manuel Vilas-Varela − *Centro Singular de Investigación en Química Biolóxica e Materiais Moleculares (CiQUS) and Departamento de Química Orgánica, Universidade de Santiago de Compostela, 15782 Santiago de Compostela, Spain*

Martina Corso − *Donostia International Physics Center, 20018 San Sebastián, Spain; Centro de Fisica de Materiales CFM/MPC, CSIC-UPV/EHU, 20018 San Sebastián, Spain;* orcid.org/0000-0002-8592-1284

Complete contact information is available at: https://pubs.acs.org/10.1021/acs.nanolett.1c03578

Author Contributions

⊥T.W. and S.S. contributed equally.

Author Contributions

The manuscript was written through contributions of all authors. All authors have given approval to the final version of the manuscript.

Notes

The authors declare no competing financial interest.

■ ACKNOWLEDGMENTS

We acknowledge financial support from the MCIN/AEI/10.13039/501100011033 (Grants PID2019-107338RB-C62, PID2019-107338RB-C63, PID2020-115406GB-I00, PCI2019-111933-2 (FLAG-ERA grant LEGOCHIP), and Juan de la Cierva Grant FJC2019-041202-I), the European Union's Horizon 2020 research and innovation program (FET-OPEN project SPRING, Grant No. 863098 and Marie Skłodowska-Curie Actions Individual Fellowship No. 101022150), the Xunta de Galicia (Centro Singular de Investigación de Galicia, 2019-2022, Grant ED431G2019/03), the European Regional Development Fund, the Basque Government (IT-1255-19), the Basque Government (PIBA Grant PI_2020_1_0014), the Basque Departamento de Educación through the Ph.D. scholarship No. PRE_2020_2_0049 (S.S.), the Spanish Research Council (LINKC20002). We thank Dr. Jingcheng Li for fruitful discussions.

■ REFERENCES

(1) Han, W.; Kawakami, R. K.; Gmitra, M.; Fabian, J. Graphene Spintronics. *Nat. Nanotechnol.* **2014**, *9* (10), 794−807.

(2) Yazyev, O. V.; Katsnelson, M. I. Magnetic Correlations at Graphene Edges: Basis for Novel Spintronics Devices. *Phys. Rev. Lett.* **2008**, *100* (4), 047209.

(3) Pisani, L.; Chan, J. A.; Montanari, B.; Harrison, N. M. Electronic Structure and Magnetic Properties of Graphitic Ribbons. *Phys. Rev. B: Condens. Matter Mater. Phys.* **2007**, *75* (6), 064418.

(4) Cui, P.; Zhang, Q.; Zhu, H.; Li, X.; Wang, W.; Li, Q.; Zeng, C.; Zhang, Z. Carbon Tetragons as Definitive Spin Switches in Narrow Zigzag Graphene Nanoribbons. *Phys. Rev. Lett.* **2016**, *116* (2), 026802.

(5) Fernández-Rossier, J.; Palacios, J. J. Magnetism in Graphene Nanoislands. *Phys. Rev. Lett.* **2007**, *99* (17), 177204.

(6) Lieb, E. H. Two Theorems on the Hubbard Model. *Phys. Rev. Lett.* **1989**, *62* (10), 1201−1204.

(7) Su, J.; Telychko, M.; Song, S.; Lu, J. Triangulenes: From Precursor Design to On-Surface Synthesis and Characterization. *Angew. Chem.* **2020**, *132* (20), 7730−7740.

(8) Wang, W. L.; Yazyev, O. V.; Meng, S.; Kaxiras, E. Topological Frustration in Graphene Nanoflakes: Magnetic Order and Spin Logic Devices. *Phys. Rev. Lett.* **2009**, *102* (15), 157201.

(9) Ezawa, M. Metallic Graphene Nanodisks: Electronic and Magnetic Properties. *Phys. Rev. B: Condens. Matter Mater. Phys.* **2007**, *76* (24), 245415.

(10) Li, J.; Sanz, S.; Corso, M.; Choi, D. J.; Peña, D.; Frederiksen, T.; Pascual, J. I. Single Spin Localization and Manipulation in Graphene Open-Shell Nanostructures. *Nat. Commun.* **2019**, *10* (1), 200.

(11) Konishi, A.; Hirao, Y.; Nakano, M.; Shimizu, A.; Botek, E.; Champagne, B.; Shiomi, D.; Sato, K.; Takui, T.; Matsumoto, K.; Kurata, H.; Kubo, T. Synthesis and Characterization of Teranthene: A Singlet Biradical Polycyclic Aromatic Hydrocarbon Having Kekulé Structures. *J. Am. Chem. Soc.* **2010**, *132* (32), 11021−11023.

(12) Wang, S.; Talirz, L.; Pignedoli, C. A.; Feng, X.; Müllen, K.; Fasel, R.; Ruffieux, P. Giant Edge State Splitting at Atomically Precise Graphene Zigzag Edges. *Nat. Commun.* **2016**, *7* (1), 11507.

(13) Kolmer, M.; Steiner, A.-K.; Izydorczyk, I.; Ko, W.; Engelund, M.; Szymonski, M.; Li, A.-P.; Amsharov, K. Rational Synthesis of Atomically Precise Graphene Nanoribbons Directly on Metal Oxide Surfaces. *Science* **2020**, *369* (6503), 571−575.

(14) Song, S.; Su, J.; Telychko, M.; Li, J.; Li, G.; Li, Y.; Su, C.; Wu, J.; Lu, J. On-Surface Synthesis of Graphene Nanostructures with π-Magnetism. *Chem. Soc. Rev.* **2021**, *50* (5), 3238−3262.

(15) Sun, Q.; Mateo, L. M.; Robles, R.; Ruffieux, P.; Lorente, N.; Bottari, G.; Torres, T.; Fasel, R. Inducing Open-Shell Character in Porphyrins through Surface-Assisted Phenalenyl π-Extension. *J. Am. Chem. Soc.* **2020**, *142* (42), 18109−18117.

(16) Zhao, Y.; Jiang, K.; Li, C.; Liu, Y.; Xu, C.; Zheng, W.; Guan, D.; Li, Y.; Zheng, H.; Liu, C.; Luo, W.; Jia, J.; Zhuang, X.; Wang, S. Precise Control of π-Electron Magnetism in Metal-Free Porphyrins. *J. Am. Chem. Soc.* **2020**, *142* (43), 18532−18540.

(17) Jacobse, P. H.; McCurdy, R. D.; Jiang, J.; Rizzo, D. J.; Veber, G.; Butler, P.; Zuzak, R.; Louie, S. G.; Fischer, F. R.; Crommie, M. F. Bottom-up Assembly of Nanoporous Graphene with Emergent Electronic States. *J. Am. Chem. Soc.* **2020**, *142* (31), 13507−13514.

(18) Zheng, Y.; Li, C.; Xu, C.; Beyer, D.; Yue, X.; Zhao, Y.; Wang, G.; Guan, D.; Li, Y.; Zheng, H.; Liu, C.; Liu, J.; Wang, X.; Luo, W.; Feng, X.; Wang, S.; Jia, J. Designer Spin Order in Diradical Nanographenes. *Nat. Commun.* **2020**, *11* (1), 6076.

(19) Zheng, Y.; Li, C.; Zhao, Y.; Beyer, D.; Wang, G.; Xu, C.; Yue, X.; Chen, Y.; Guan, D.-D.; Li, Y.-Y.; Zheng, H.; Liu, C.; Luo, W.; Feng, X.; Wang, S.; Jia, J. Engineering of Magnetic Coupling in Nanographene. *Phys. Rev. Lett.* **2020**, *124* (14), 147206.

(20) Mishra, S.; Beyer, D.; Berger, R.; Liu, J.; Gröning, O.; Urgel, J. I.; Müllen, K.; Ruffieux, P.; Feng, X.; Fasel, R. Topological Defect-Induced Magnetism in a Nanographene. *J. Am. Chem. Soc.* **2020**, *142* (3), 1147−1152.

(21) Li, J.; Sanz, S.; Castro-Esteban, J.; Vilas-Varela, M.; Friedrich, N.; Frederiksen, T.; Peña, D.; Pascual, J. I. Uncovering the Triplet Ground State of Triangular Graphene Nanoflakes Engineered with Atomic Precision on a Metal Surface. *Phys. Rev. Lett.* **2020**, *124* (17), 177201.

(22) Wang, X.; Sun, G.; Routh, P.; Kim, D.-H.; Huang, W.; Chen, P. Heteroatom-Doped Graphene Materials: Syntheses, Properties and Applications. *Chem. Soc. Rev.* **2014**, *43* (20), 7067−7098.

(23) Gonzalez-Herrero, H.; Gomez-Rodriguez, J. M.; Mallet, P.; Moaied, M.; Palacios, J. J.; Salgado, C.; Ugeda, M. M.; Veuillen, J.-Y.; Yndurain, F.; Brihuega, I. Atomic-Scale Control of Graphene Magnetism by Using Hydrogen Atoms. *Science* **2016**, *352* (6284), 437−441.

(24) Friedrich, N.; Brandimarte, P.; Li, J.; Saito, S.; Yamaguchi, S.; Pozo, I.; Peña, D.; Frederiksen, T.; Garcia-Lekue, A.; Sánchez-Portal, D.; Pascual, J. I. Magnetism of Topological Boundary States Induced

by Boron Substitution in Graphene Nanoribbons. *Phys. Rev. Lett.* **2020**, *125* (14), 146801.
(25) Babar, R.; Kabir, M. Ferromagnetism in Nitrogen-Doped Graphene. *Phys. Rev. B: Condens. Matter Mater. Phys.* **2019**, *99* (11), 115442.
(26) Błoński, P.; Tuček, J.; Sofer, Z.; Mazánek, V.; Petr, M.; Pumera, M.; Otyepka, M.; Zbořil, R. Doping with Graphitic Nitrogen Triggers Ferromagnetism in Graphene. *J. Am. Chem. Soc.* **2017**, *139* (8), 3171−3180.
(27) Clair, S.; de Oteyza, D. G. Controlling a Chemical Coupling Reaction on a Surface: Tools and Strategies for On-Surface Synthesis. *Chem. Rev.* **2019**, *119* (7), 4717−4776.
(28) Sun, Q.; Yao, X.; Gröning, O.; Eimre, K.; Pignedoli, C. A.; Müllen, K.; Narita, A.; Fasel, R.; Ruffieux, P. Coupled Spin States in Armchair Graphene Nanoribbons with Asymmetric Zigzag Edge Extensions. *Nano Lett.* **2020**, *20* (9), 6429−6436.
(29) Ruffieux, P.; Wang, S.; Yang, B.; Sánchez-Sánchez, C.; Liu, J.; Dienel, T.; Talirz, L.; Shinde, P.; Pignedoli, C. A.; Passerone, D.; Dumslaff, T.; Feng, X.; Müllen, K.; Fasel, R. On-Surface Synthesis of Graphene Nanoribbons with Zigzag Edge Topology. *Nature* **2016**, *531* (7595), 489−492.
(30) Liu, J.; Mishra, S.; Pignedoli, C. A.; Passerone, D.; Urgel, J. I.; Fabrizio, A.; Lohr, T. G.; Ma, J.; Komber, H.; Baumgarten, M.; Corminboeuf, C.; Berger, R.; Ruffieux, P.; Müllen, K.; Fasel, R.; Feng, X. Open-Shell Nonbenzenoid Nanographenes Containing Two Pairs of Pentagonal and Heptagonal Rings. *J. Am. Chem. Soc.* **2019**, *141* (30), 12011−12020.
(31) Mateo, L. M.; Sun, Q.; Liu, S.; Bergkamp, J. J.; Eimre, K.; Pignedoli, C. A.; Ruffieux, P.; Decurtins, S.; Bottari, G.; Fasel, R.; Torres, T. On-Surface Synthesis and Characterization of Triply Fused Porphyrin−Graphene Nanoribbon Hybrids. *Angew. Chem., Int. Ed.* **2020**, *59* (3), 1334−1339.
(32) Mishra, S.; Beyer, D.; Eimre, K.; Ortiz, R.; Fernández-Rossier, J.; Berger, R.; Gröning, O.; Pignedoli, C. A.; Fasel, R.; Feng, X.; Ruffieux, P. Collective All-Carbon Magnetism in Triangulene Dimers. *Angew. Chem., Int. Ed.* **2020**, *59* (29), 12041−12047.
(33) Lawrence, J.; Brandimarte, P.; Berdonces-Layunta, A.; Mohammed, M. S. G.; Grewal, A.; Leon, C. C.; Sánchez-Portal, D.; de Oteyza, D. G. Probing the Magnetism of Topological End States in 5-Armchair Graphene Nanoribbons. *ACS Nano* **2020**, *14* (4), 4499−4508.
(34) Sánchez-Grande, A.; Urgel, J. I.; Veis, L.; Edalatmanesh, S.; Santos, J.; Lauwaet, K.; Mutombo, P.; Gallego, J. M.; Brabec, J.; Beran, P.; Nachtigallová, D.; Miranda, R.; Martín, N.; Jelínek, P.; Écija, D. Unravelling the Open-Shell Character of Peripentacene on Au(111). *J. Phys. Chem. Lett.* **2021**, *12* (1), 330−336.
(35) Su, X.; Li, C.; Du, Q.; Tao, K.; Wang, S.; Yu, P. Atomically Precise Synthesis and Characterization of Heptauthrene with Triplet Ground State. *Nano Lett.* **2020**, *20* (9), 6859−6864.
(36) Mishra, S.; Beyer, D.; Eimre, K.; Kezilebieke, S.; Berger, R.; Gröning, O.; Pignedoli, C. A.; Müllen, K.; Liljeroth, P.; Ruffieux, P.; Feng, X.; Fasel, R. Topological Frustration Induces Unconventional Magnetism in a Nanographene. *Nat. Nanotechnol.* **2020**, *15* (1), 22−28.
(37) Mishra, S.; Yao, X.; Chen, Q.; Eimre, K.; Gröning, O.; Ortiz, R.; Di Giovannantonio, M.; Sancho-García, J. C.; Fernández-Rossier, J.; Pignedoli, C. A.; Müllen, K.; Ruffieux, P.; Narita, A.; Fasel, R. Large Magnetic Exchange Coupling in Rhombus-Shaped Nanographenes with Zigzag Periphery. *Nat. Chem.* **2021**, *13*, 581.
(38) Rizzo, D. J.; Veber, G.; Jiang, J.; McCurdy, R.; Cao, T.; Bronner, C.; Chen, T.; Louie, S. G.; Fischer, F. R.; Crommie, M. F. Inducing Metallicity in Graphene Nanoribbons via Zero-Mode Superlattices. *Science* **2020**, *369* (6511), 1597−1603.
(39) Lawrence, J.; Berdonces-Layunta, A.; Edalatmanesh, S.; Castro-Esteban, J.; Wang, T.; Mohammed, M. S. G.; Vilas-Varela, M.; Jelinek, P.; Peña, D.; de Oteyza, D. G. *Circumventing the Stability Problems of Graphene Nanoribbon Zigzag Edges*. arXiv. 2021, 2107.12754. https://arxiv.org/abs/2107.12754 (accessed November 25, 2021).
(40) de Oteyza, D. G.; García-Lekue, A.; Vilas-Varela, M.; Merino-Díez, N.; Carbonell-Sanromà, E.; Corso, M.; Vasseur, G.; Rogero, C.; Guitián, E.; Pascual, J. I.; Ortega, J. E.; Wakayama, Y.; Peña, D. Substrate-Independent Growth of Atomically Precise Chiral Graphene Nanoribbons. *ACS Nano* **2016**, *10* (9), 9000−9008.
(41) Berdonces-Layunta, A.; Lawrence, J.; Edalatmanesh, S.; Castro-Esteban, J.; Wang, T.; Mohammed, M. S. G.; Colazzo, L.; Peña, D.; Jelínek, P.; de Oteyza, D. G. Chemical Stability of (3,1)-Chiral Graphene Nanoribbons. *ACS Nano* **2021**, *15* (3), 5610−5617.
(42) Jelínek, P. High Resolution SPM Imaging of Organic Molecules with Functionalized Tips. *J. Phys.: Condens. Matter* **2017**, *29* (34), 343002.
(43) Soler, J. M; Artacho, E.; Gale, J. D; García, A.; Junquera, J.; Ordejón, P.; Sánchez-Portal, D. *Phys. Condens. Matter.* **2002**, *14*, 2745.
(44) Perdew, J. P.; Burke, K.; Ernzerhof, M. *Phys. Rev. Lett.* **1996**, *77*, 3865.
(45) Kondo, J. Resistance Minimum in Dilute Magnetic Alloys. *Prog. Theor. Phys.* **1964**, *32* (1), 37−49.
(46) Frota, H. O. Shape of the Kondo Resonance. *Phys. Rev. B: Condens. Matter Mater. Phys.* **1992**, *45* (3), 1096−1099.
(47) Nagaoka, K.; Jamneala, T.; Grobis, M.; Crommie, M. F. Temperature Dependence of a Single Kondo Impurity. *Phys. Rev. Lett.* **2002**, *88* (7), 077205.
(48) Merino-Díez, N.; Li, J.; Garcia-Lekue, A.; Vasseur, G.; Vilas-Varela, M.; Carbonell-Sanromà, E.; Corso, M.; Ortega, J. E.; Peña, D.; Pascual, J. I.; de Oteyza, D. G. Unraveling the Electronic Structure of Narrow Atomically Precise Chiral Graphene Nanoribbons. *J. Phys. Chem. Lett.* **2018**, *9* (1), 25−30.
(49) Ternes, M. Spin Excitations and Correlations in Scanning Tunneling Spectroscopy. *New J. Phys.* **2015**, *17* (6), 063016.
(50) (https://github.com/dipc-cc/hubbard).
(51) DiLullo, A.; Chang, S.-H.; Baadji, N.; Clark, K.; Klöckner, J.-P.; Prosenc, M.-H.; Sanvito, S.; Wiesendanger, R.; Hoffmann, G.; Hla, S.-W. Molecular Kondo Chain. *Nano Lett.* **2012**, *12* (6), 3174−3179.

https://doi.org/10.1021/acs.nanolett.1c03578
Nano Lett. 2022, 22, 164−171